HYDROMAGNETIC HYBRID NANOFLUID FLOW AND MASS TRANSFER FROM A STRETCHING SURFACE IN POROUS MEDIA WITH NAVIER SLIP AND CHEMICAL REACTION EFFECTS

U. S. Mahabaleshwar[1], O. Anwar Bég[2], Dumitru Baleanu[3]&T. Anusha[4*]

[1]Department of Mathematics, Davangere University, Shivagangothri, Davangere, 577 007, INDIA, Email: u.s.m@davangereuniversity.ac.in
[2]School of Science, Engineering and Environment, Aeronautical and Mechanical Engineering, University of Salford, Manchester, U.K, Email: O.A.Beg@salford.ac.uk
[3]Department of Mathematics, Cankaya University, Turkey & Institute of Space Sciences, Romania, E-mail: Dumitru.baleanu@gmail.com
[4]Department of Mathematics, Davangere University, Shivagangothri, Davangere, 577 007, INDIA, Email: anushat.math@gmail.com*

***** *Corresponding author*: *anushat.math@gmail.com [Anusha T], Phone: +917619224655.*

Acknowledgements

The author Anusha T. is thankful to Council of Scientific and Industrial Research (CSIR), New Delhi, INDIA for financial support in the form of Junior Research Fellowship(JRF): File No. 09/1207(0003)/2020-EMR-I.

Abstract

Hybrid nanofluids (HNFs) comprise combinations of different nanoparticles suspended in base fluids. Applications of such nanofluids are growing in the areas of energy and biomedical engineering including smart (functional) coatings. Motivated by these developments, the present article examines theoretically the magnetohydrodynamic (MHD) coating boundary layer flow of HNFs from a stretching surface under a transverse magnetic field in porous media with chemically reactive nanoparticles. Darcy's law is deployed. Both first and second order momentum slip is included as is solutal slip. The transformed boundary value problem is solved analytically. Closed form solutions for velocity are derived in terms of exponential functions and for the concentration field in terms of incomplete Gamma functions by the application of the Laplace transformation technique. The influence of selected parameters e.g. suction/injection, magnetic field and slip parameters on velocity and concentration distributions are visualized graphically. Concentration magnitudes are elevated with stronger magnetic field whereas they are suppressed with greater wall solutal slip. Magnetic field suppresses velocity and increases hydrodynamic boundary layer thickness. The flow is accelerated with reduction in inverse Darcy number and stronger suction leads to a decrease in skin friction. The analysis provides a good foundation for further investigations using numerical methods.

Keywords: Ordinary differential equation, incomplete Gamma function, Laplace transformation, analytical solution, Darcy number.

1. INTRODUCTION

In recent years nanofluids [1] have mobilized significant interest owing to their superior performance in many technologies including bio-microfluidics, aerospace, environmental and energy systems [2-8]. Nanofluids are colloidal suspensions engineered at the nanoscale and comprise conventional base fluids e. g. water, doped with metallic (e. g. zinc, titanium, iron, copper, gold, silver and their oxides) or non-metallic (carbon based e. g. silicates, graphene, diamond etc) nanoparticles (spheres, rods, tubes, shells, ellipsoids etc). *Magnetic nanofluids* [9] are another subset of modern nanofluids which feature electrically conducting nanoparticles and invoke magnetohydrodynamic (MHD) [10] effects, allowing thermal/mass transport to be manipulated via external magnetic fields. These have been examined in many applications and recent works in this regard include Bég *et al.* [11] (smart orthopaedic magnetic nanofluid films) and Li *et al.*[12] (magnet core/shell $L1_0$-CoPt/Pt-water nanofluids in Proton exchange membrane fuel cells).

Functional nano materials, of which magnetic nanofluids are an example, offer improved corrosion and abrasion resistance in the new generation of "smart nano-coatings" [13]. The manufacturing of such nanofluid smart coatings frequently involves the stretching of a sheet over a metallic substrate or enrobing. This area offers many interesting features which can be studied with fluid mechanics and applied mathematical methods and has therefore stimulated considerable interest in recent years. Mahabaleshwar *et al.* [14] investigated the hydromagnetic nanofluid flow from an extending sheet with wall mass flux (suction) observing that an increment in Chandrasekhar number (square of the Hartmann number) strongly decelerates the flow and furthermore that a substantial modification in flow is induced with different nanoparticle types. Aneja *et al.* [15] used a variational finite element method and Buongiorno's two-component nanoscale model to compute the impact of non-uniform magnetic field on aqueous nanofluid stretching sheet flow containing motile gyrotactic micro-organisms from a tilted surface with Ohmic dissipation (Joule heating) as a model of smart solar coatings. They observed that strong retardation in the flow is produced with greater inclination and magnetic field strength whereas temperatures, motile micro-organism density number (bioconvection species concentration) and nanoparticle concentration are boosted. Hamad [16] derived closed-form solutions for magnetic nanofluid boundary layer flow from a semi-infinite vertical

stretching surface under static transverse magnetic field, studying in detail the influence of solid volume fraction of nanoparticles and magnetic field on Nusselt number and skin friction coefficient. Hsiao [17] used the Keller box finite difference scheme to simulate the hydromagnetic boundary layer flow with Joule heating and viscous dissipation in micropolar nanofluid flow from a stretching sheet. He found that stronger magnetic parameter depresses velocity magnitudes and Nusselt number whereas the opposite trend is induced in shear stress, wall couple stress (micro-rotation gradient), temperature and nanoparticle concentration.

The above studies were generally confined to unitary magnetic nanofluids, in which a single magnetic nanoparticle is deployed in the base fluid. However, engineers have also explored combinations of different nanoparticles in base fluids, and these are known as *hybrid nanofluids (HNFs)*. It has been observed from both theoretical and experimental studies [18-20] that hybrid nanofluids achieve even better thermal and mass diffusion enhancement characteristics than conventional (unitary i.e. single nanoparticle material) nanofluids. Applications of hybrid nanofluids have been explored in biocompatible nano-hemodynamics, mechanical heat sinks, helical and plate heat exchangers and also smart thin film coatings. Examples of hybrid nanofluids studied include $TiO_2 - CuO$ /Ethylene glycol nanofluid [21] and aqueous silica–alumina hybrid nanofluid [22]. Lund *et al*. [23] showed that the rate of heat transfer (Nusselt number) and nanoparticle mass transfer (Sherwood number) in hybrid nanofluids is higher than normal nanofluids. Hayat and Nadeem [24] examined three-dimensional rotating flow of an aqueous $Ag - CuO$ hybrid nanofluid, also noting superior performance of the hybrid mixture compared with unitary nanofluids. Other studies have considered combinations of graphite and zinc diamond nanoparticles in hybrid designs. Prakash et al. [25] investigated electro-osmotic propulsion of hybrid nanofluids (titania, alumina or copper metallic nanoparticles in water) in a deformable conduit using All these studies confirm that improved thermo-mass diffusion performance is attained with hybrid nanofluids. *Hybrid nanofluid transport from stretching sheets,* of relevance to materials processing systems has also been examined by a variety of researchers. Aly and Pop [26] computed the magnetohydrodynamic flow of aqueous hybrid nanofluid based from shrinking/stretching sheets, considering dual solutions. Khan et al. [27] studied hybrid nanofluid $TiO_2 - Cu / H_2O$ stretching sheet flow, observing superior performance to unitary Cu -Water nanofluid. Olatundun and

Makinde [28] computed the Blasius flow hybrid $Al_2O_3 - Cu$ water nanofluid from a convectively heated surface, also considering shape factor effects and studying five different geometries of nanoparticles (spherical, bricks, cylindrical, platelets and blades). They noted that Nusselt numbers are greater for hybrid nanofluid ($Cu - Al_2O_3$ /Water) relative to unitary nanofluid (Al_2O_3 /Water) and the blade shaped nanoparticles also produce the best thermal enhancement.

In many *coating applications*, a porous medium can be deployed to achieve improved flow control during deposition processes [29]. The most popular approach for porous media flows is the classical Darcian model which is valid for *low Reynolds number, viscous-dominated flows*, which characterize numerous manufacturing coating flows. The implementation of porous media is useful in stretching flows where, as explained earlier, the nano-coating is extended over a substrate (e.g. metallic component). Porous media also feature extensively in biomedical applications. Some interesting studies of magnetic nanofluid flows in porous media include Pal and Mandal [30] who used a Runge–Kutta–Fehlberg method with shooting technique to compute copper-water nanofluid stagnation flow from a contracting/extending surface in Darcian porous media. Bég *et al*. [31] used a Chebychev spectral collocation code to simulate the Von Karman swirling bio-convective nanofluid transport from a rotating disk in a Darcian porous medium. They showed that radial skin friction is elevated with positive values of the power law stretching parameter, whereas it is decreased with negative values and the converse response is computed for circumferential skin friction, nanoparticle mass transfer rate and motile micro-organism density number gradient. Manh *et al.* [32] deployed a control volume finite element method (CVFEM) to simulate hydromagnetic nanoparticle (Fe_3O_4 + MWCNT) aqueous nanofluid hydromagnetic flow in a non-Darcy porous medium with radiative flux and buoyancy effects. They noted that average Nusselt number is boosted markedly with thermal buoyancy effect (Rayleigh number) and permeability effect (Darcy number) whereas it is suppressed with magnetic Hartmann number and furthermore strong damping in the velocity field is induced with higher Hartmann number. More recently Venkatadri *et al.* [33] deployed a Newton Fehlberg iteration technique to compute the *phase change magnetic hybrid nanofluid coating* flow from an exponentially shrinking/stretching porous sheet in porous media with radiative heat flux.

While most nanofluid studies have considered thermal aspects, very few have considered solely the momentum and mass diffusion in nano-coating boundary layer flow. In mass transfer coating operations, chemical reactions frequently occur, and these can be manipulated to produce specific characteristics in nano-coatings which are critical for their subsequent selection in different applications. This is particularly of relevance to the sol-gel method of nano-coating synthesis wherein colloidal nanoparticles are generated from the liquid phase. This chemical method is based on hydrolysis or condensation reactions and it has been shown [34] that with carefully organized reactants, nanosized particles precipitate and produce coatings which exhibit exceptional advantages such as versatility and easy shaping. Chemical reactions may be constructive or destructive. They may also be homogenous or heterogenous. Mathematical models of reactive coating flows have therefore received some attention in recent years. Akyildiz et al. [36] analyzed the diffusion of chemically reactive species of a non-Newtonian fluid in a porous medium from a stretching sheet, deploying the Brouwer fixed point theorem to establish the existence of different solutions. They studied nth order homogenous chemical reaction effects and employed a Darcian model, noting that fluid concentration increases with an increase in the reaction-order parameter for positive index of reaction (destructive) whereas the opposite behavior arises for negative exponent (generative reaction). Abad *et al.* [37] used an artificial neural network and particle swarm optimization to simulate the reactive hybrid $Al_2O_3 - Cu$ - water (Aluminium oxide-Copper-water) nanofluid flow from a cylindrical bluff-body embedded in porous media and featuring homogenous and heterogeneous chemical reactions. They observed that elevation in volume fraction increases chemical species production whereas greater interfacial area suppresses mass transfer of nanoparticles. Uddin *et al.* [38] used Lie group algebraic methods and MAPLE quadrature to analyze the two-dimensional hydromagnetic viscous incompressible free convective boundary layer flow of an electrically conducting, chemically reacting nanofluid from a convectively heated permeable vertical surface is presented. They observed that velocity and temperature is enhanced with increasing order of chemical reaction whereas nanoparticle volume fraction (concentration) is reduced.

In numerous materials fabrication systems slip effects are known to arise at the wall (e.g. conveyor belt). Slip is generally associated with molecular dynamics in the fluid near the boundary and leads to non-adherence of coatings to substrates. These effects can significantly

alter heat, mass and momentum characteristics in coating extrusion. The boundary value problems associated with such flows have stimulated some interest in recent years and in addition to momentum slip, thermal jump (slip) and also mass slip effects have also been addressed. Mabood *et al.* [39] used a Bellman-Kalaba quasi-linearization technique to study the unsteady flow with velocity, thermal and solutal slip effects on radiative hydromagnetic flow from a porous extending sheet. Bég *et al*. [40] used the PSPICE network electro thermal code to compute the slip effects on Von Karman swirling hydromagnetic convective flow from a rotating disk with wall transpiration and radiative heat transfer. Mahabaleshwar *et al.*[41] analyzed the stretching sheet convective-radiative flow of a short memory viscoelastic fluid with Navier wall slip in Darcian porous media. Mahabaleshwar *et al*. [42] modeled the problem of axisymmetric flow over stretching sheet in the presence slip; since this boundary value problem did not yield analytical solutions it was therefore solved with a semi-numerical method known as the differential transform method (DTM) in combination with Padé approximations to accelerate convergence. Nanofluid slip boundary layer flows have been investigated by Hakeem*et al.* [43] who considered second order slip in radiative magnetic nanofluid flow from both extending and contracting sheets. Shukla *et al.* [44] obtained homotopy solutions for entropy generation in time-dependent stagnation slip flow of a reactive nanofluid in the presence of both electrical and magnetic fields. Further studies include Govindaraju *et al*. [45] (for silver-water nanofluids), Bhatti*et al.* [45] (for magnetic Fe_3O_4-water-based nanofluid with quadratic sheet stretching and cross diffusion effects), Babu and Sandeep [46] (for water-graphene nanofluid when compared with water-magnetite nanofluids), Uddin *et al.* [48] (for magnetohydrodynamic bioconvection nanofluid coating flows), Tulu and Ibrahim [49] (for carbon nanotube-ethylene glycol nanofluid swirling disk flow) and Shukla *et al.* [49] (for entropy generation in magnetic silver/zinc nanofluid external coating boundary layers on a vertical cylinder). Although in many boundary value problems, numerical methods are frequently utilized, it is also possible to use the method of Laplace transformation (LT) to derive analytical solutions for nanofluid coating boundary layer flows. Saleh *et al*. [50] investigated convection in CNT (carbon nanotube) nanofluids with cancer tumor treatment applications using Laplace transforms. Ebaid and Sharif [51] studied thermo-magnetic CNT nanofluid flow with Laplace transform methods. Bhullar *et al.* [52] has

provided a detailed appraisal of applications and properties of Laplace transformation methods in fluid dynamics and other areas of engineering sciences.

In the present article, a mathematical model is developed for the convective momentum and mass transfer in magnetohydrodynamic hybrid nanofluid flow from a stretching surface adjacent to a porous medium with chemical reaction effects. Navier's slip conditions in addition to thermal and mass (nanoparticle) wall slip are also included. Closed form solutions for velocity are derived in terms of exponential functions and for the concentration field in terms of incomplete Gamma functions by the application of the Laplace transformation technique. The influence of selected parameters e.g. suction/injection, magnetic field and slip parameters on velocity and concentration distributions are visualized graphically. The computations are relevant to smart functional magnetic nanofluid coating applications.

2. MATHEMATICAL MODEL

Consider the incompressible Newtonian HNF flow due to a linearly stretched semi-infinite sheet (coating) embedded in porous media with mass transpiration and chemical reaction. Navier's momentum slip [54] and also nanoparticle concentration (solutal) slip are included. The sheet is stretched in the *x*-direction and the *y*-axis is perpendicular to the plane of stretching. A uniform magnetic field with strength B_0 is applied in the *y*-direction. Magnetic induction effects are negated (magnetic Reynolds number is sufficiently small such that the magnetic field is not distorted). The porous medium is non-deformable, assumed to be *isotropic* (constant permeability in all directions) and homogenous and Darcy's law is assumed. The nanofluid is also assumed to be dilute and a first order homogenous destructive chemical reaction is considered. Under these approximations and the boundary-layer assumption, the equations of conservation of mass and momentum and concentration (nanoparticle species) may be presented as the following system of coupled, nonlinear PDE's:

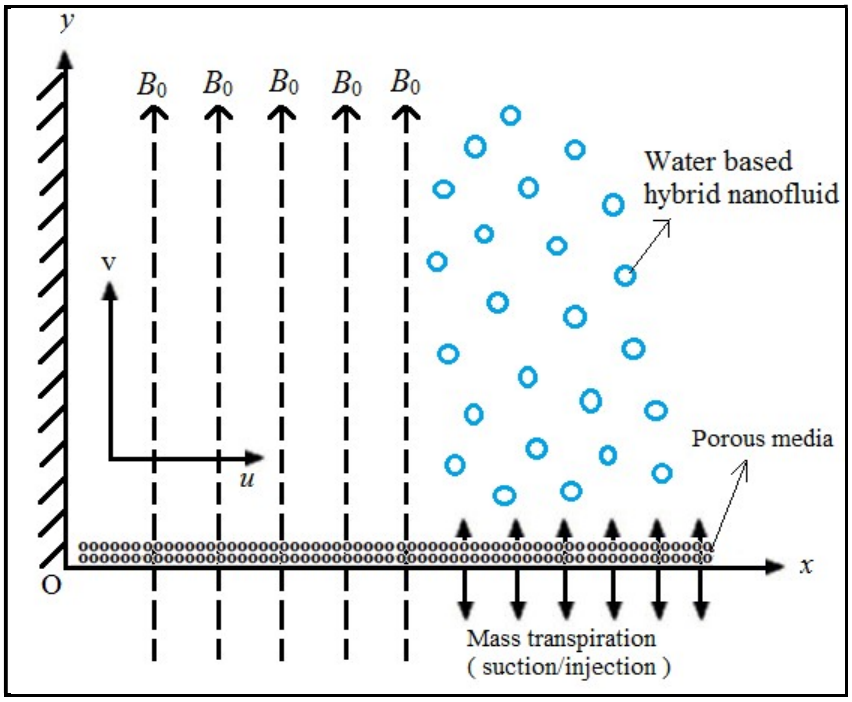

Fig. 1: Schematic of reactive MHD nanofluid coating boundary layer flow in porous media.

$$u_x + \mathrm{v}_y = 0, \tag{1}$$

$$uu_x + \mathrm{v}u_y = \nu_{eff} u_{yy} - \frac{\sigma_{hnf} B_0^2}{\rho_{hnf}} u - \frac{\mu_{hnf}}{\kappa \rho_{hnf}} u = 0, \tag{2}$$

$$uC_x + \mathrm{v}C_y = D_B C_{yy} - k_c \left(C - C_\infty\right), \tag{3}$$

The associated B.C.s are prescribed at the wall (sheet) and in the free stream as:

$$u\left(x,0\right) = ax + u_{slip},\ \mathrm{v}\left(x,0\right) = \mathrm{v}_w,\ u\left(x,\infty\right) \to 0, \tag{4a}$$

$$C\left(x,0\right) = C_w + K_1 C_y\left(x,0\right),\ C\left(x,\infty\right) \to C_\infty \quad , \tag{4b}$$

In Eqn. (4a), u_{slip} is the wall slip velocity which is taken as:

$$u_{slip} = \frac{2}{3}\left[\frac{3-\gamma m^3}{\gamma} - \frac{3\left(1-m^2\right)}{2K}\right]\alpha u_y - \frac{1}{4}\left[m^4 + \frac{2}{K^2}\left(1-m^2\right)\right]\alpha^2 u_{yy}, \tag{5}$$

This may be re-written as follows:

$$u_{slip} = L_1 u_y + L_2 u_{yy}, \tag{6}$$

Here, $0 \le \gamma \le 1$ is the coefficient of momentum accommodation, further the molecular free path α is positive, which implies that $L_1 \ge 0$ and $L_2 \le 0$. m is the minimum value among the numbers $1/K$ and 1 which clearly implies $0 \le m \le 1$ for any K, where K is the Knudsen number (ratio of the molecular mean free path length to a representative physical length scale) which is valid for arbitrary values as elaborated in Wu [55]. Additionally, the applications of Knudsen number can be found in [54]. The primitive form of the boundary layer equations is challenging to solve. It is therefore pertinent to introduce scaling transformations. Consider suitable similarity transformations with stream function which following Hamad [16] may be defined as follows:

$$\psi = \sqrt{a\nu_f}\, x f(\eta) \qquad \text{and} \qquad \eta = \sqrt{\frac{a}{\nu_f}}\, y, \tag{7}$$

The velocities along x- and y- directions respectively emerge in terms of these transformations as:

$$u = a x f_\eta(\eta) \quad \text{and} \quad \mathrm{v} = -\sqrt{a\nu_f}\, f(\eta), \tag{8}$$

Further the transformation for concentration is taken as:

$$\phi(\eta) = \frac{C - C_\infty}{C_w - C_\infty}, \tag{9}$$

On applying (7) to (9) in the momentum and species diffusion boundary layer Eqns. (2) and (3) we obtain:

$$\delta_1 \Lambda f_{\eta\eta\eta} + \delta_1 \left(f f_{\eta\eta} - f_\eta^2 \right) - \left(\delta_3 M + \delta_2 Da^{-1} \right) f_\eta = 0, \tag{10}$$

$$\phi_{\eta\eta} + Scf\, \phi_\eta = \beta Sc \phi, \tag{11}$$

The B.C.s (4a) and (4b) become:

$$f(0)=V_C,\ f_\eta(0)=1+S_1 f_{\eta\eta}(0)+S_2 f_{\eta\eta\eta}(0),\ f_\eta(\infty)=0, \tag{12a}$$

$$\phi(0)=1+S_3\phi_\eta(0),\ \phi(\infty)=0, \tag{12b}$$

Here, all physical parameters are defined in the nomenclature and are in accordance with Andersson and Bech [56], Siddheshwar *et al.* [57] and Andersson *et al.* [58].

3. Exact solution of Momentum Field

The exact solutions for the momentum Eqn. (0) with the relevant boundary conditions from (12a,b) can be expressed in the form:

$$f(\eta)=A+Bexp(-\lambda\eta), \tag{13}$$

On using B.Cs (12a) to determine the constants, the solution will become:

$$f(\eta)=V_C-\frac{\left[1-exp(-\lambda\eta)\right]}{\lambda\left(S_2\lambda^2-S_1\lambda-1\right)}, \tag{14}$$

The wall skin friction (dimensionless surface shear stress) is given by:

$$-f_{\eta\eta}(0)=-\frac{\lambda}{S_2\lambda^2-S_1\lambda-1}, \tag{15}$$

Here the unknown λ can be determined from the following equation which is obtained by using equation (13) in (10):

$$\begin{aligned}\delta_1\Lambda S_2\lambda^4-\delta_1\left(\Lambda S_1+V_C S_2\right)\lambda^3-\left(\delta_1\Lambda-\delta_1 V_C S_1+\delta_3 M S_2+\delta_2 Da^{-1}S_2\right)\lambda^2 \\ +\left(\delta_1 V_C+\delta_3 M S_1+\delta_2 Da^{-1}S_1\right)\lambda+\left(\delta_1+\delta_3 M+\delta_2 Da^{-1}\right)=0\end{aligned} \tag{16}$$

Next, we implement the method of Laplace transforms to find the simple exact analytical solution in terms of incomplete gamma function.

4. SOLUTION FOR MASS TRANSFER PROBLEM:

Using Eqn. (13) in the dimensionless nanoparticle species conservation Eqn. (7) the mass transfer Eqn. is rendered as follows:

$$\phi_{\eta\eta} + Sc\left[A + Bexp\left(-\lambda\eta\right)\right]\phi_{\eta} = \beta Sc\phi\,, \tag{17}$$

By taking the new variable $\xi = exp\left(-\lambda\eta\right)$, Eqn. (17) takes the form:

$$\xi\phi_{\xi\xi} + \left[1 - \frac{Sc}{\lambda}\left(A + B\xi\right)\right]\phi_{\xi} = \frac{\beta Sc}{\lambda^2}\frac{1}{\xi}\phi, \tag{18}$$

The B.C.s (12b) assume the form:

$$\phi\left(1\right) = 1 + S_3\phi_{\xi}\left(1\right),\ \phi\left(0\right) = 0, \tag{19}$$

Introducing the substitutions:

$$1 - \frac{ScA}{\lambda} = \chi_1,\ \ \frac{ScB}{\lambda} = \chi_2, \text{ and } \ \frac{\beta Sc}{\lambda^2} = \chi_3\,, \tag{20}$$

It follows that Eqn. (18) becomes:

$$\xi\phi_{\xi\xi} + \left[\chi_1 - \chi_2\xi\right]\phi_{\xi} = \chi_3\frac{1}{\xi}\phi\,, \tag{21}$$

To solve Eqn. (21), we deploy Laplace transformation to obtain:

$$S\left(\chi_2 - S\right)\phi_S\left(S\right) + \left[\chi_2 + S\left(\chi_1 - 2\right)\right]\phi\left(S\right) = \chi_3\int_S^{\infty}\phi\left(S\right)dS\,, \tag{22}$$

The solution of Eqn. (22) for the non-reactive species i.e. for $\beta = 0$ is:

$$\phi\left(S\right) = \frac{C}{S\left(S - \chi_2\right)^{\left(1-\chi_1\right)}} \tag{23}$$

In order to apply inverse Laplace transformations, $\chi_1 < 1$ and here $\phi\left(S\right) = L\left[\phi\left(\xi\right)\right]$ so that Eqn. (23) gives:

$$\phi\left(\xi\right) = \frac{C\xi^{-\chi_1}exp\left(\chi_2\xi\right)}{\Gamma\left[1 - \chi_1\right]}, \tag{24}$$

By applying the convolution property of Laplace transformations in Eqn. (24) gives:

$$\phi(\xi)=\frac{C}{\left(-\chi_2\right)^{(1-\chi_1)}}\frac{\Gamma\left[1-\chi_1,0,-\chi_2\xi\right]}{\Gamma\left[1-\chi_1\right]}, \tag{25}$$

Using the B.C.s in (19) to find the constant in Eqn. (25) yields:

$$\phi(\xi)=\frac{\Gamma\left[1-\chi_1,0,-\chi_2\xi\right]}{\Gamma\left[1-\chi_1,0,-\chi_2\right]+S_3 exp\left(\chi_2\right)\left(-\chi_2\right)^{(1-\chi_1)}}, \tag{26}$$

In terms of the similarity variable η Eqn. (26) becomes:

$$\phi(\eta)=\frac{\Gamma\left[1-\chi_1,0,-\chi_2 exp\left(-\lambda\eta\right)\right]}{\Gamma\left[1-\chi_1,0,-\chi_2\right]+S_3 exp\left(\chi_2\right)\left(-\chi_2\right)^{(1-\chi_1)}}. \tag{27}$$

This defines the exact analytical solution for the concentration field which in terms of incomplete gamma functions may be expressed as:

$$\phi_\eta(\eta)=\frac{\lambda\left(-\chi_2 exp\left(-\lambda\eta\right)\right)^{1-\chi_1} exp\left[\chi_2 exp\left(-\lambda\eta\right)\right]}{\Gamma\left[1-\chi_1,0,-\chi_2\right]+S_3 exp\left(\chi_2\right)\left(-\chi_2\right)^{(1-\chi_1)}}, \tag{28}$$

The Sherwood number (dimensionless mass transfer rate at the wall i.e. sheet) takes the form:

$$-\phi_\eta(0)=-\frac{\lambda\left(-\chi_2\right)^{1-\chi_1} exp\left(\chi_2\right)}{\Gamma\left[1-\chi_1,0,-\chi_2\right]+S_3 exp\left(\chi_2\right)\left(-\chi_2\right)^{(1-\chi_1)}}. \tag{29}$$

5. RESULTS AND DISCUSSION

The system of PDEs describing the hybrid nanofluid magnetic stretching sheet flow problem has been transformed into a system of nonlinear ODEs with constant coefficients by using the suitable similarity transformations for velocity and concentration. The analytical solution for velocity has been obtained in exponential form and that for the concentration field has been derived in terms of incomplete gamma function by the usage of Laplace transformation. Using

appropriate symbolic software e.g. MATLAB, the closed-form solutions can then be evaluated for different parameter values and plotted against transverse coordinate. The numerical results based on this process are visualized in **Figs. 2-7** for the influence of constant magnetic field, mass transpiration, Navier's slip and solutal slip effects. Copper-Alumina hybrid nanofluidis considered.

Fig.2 portrays the variation of transverse velocity with different values of *M* for suction case in (a) and injection case in (b) and reveals that, the transverse velocity will reduce with the increase in *M* in both cases. The same effect is evident in Fig. 3 for axial velocity. These plots indicate that the velocity boundary layer will increase in thickness with an increase in magnetic field due to the inhibiting effect of the Lorentz magnetic drag force which acts orthogonally to the applied magnetic field. This induces a strong damping effect on the boundary layer flow. Initially transverse velocity will increase rapidly and becomes constant after some value of η for both the cases, while the axial velocity initially decreases exponentially and becomes zero after some value of η. Axial velocity is always positive for both *suction and injection* cases (Fig. 3); however transverse velocity is only positive in the case of suction ($V_C = 1$) and evidently at large magnetic interaction parameter values velocity assumes negative values since blowing combined with strong Lorentz force (the effect is most prominent at high *M* values) induces flow reversal (back flow) in the boundary layer (Fig. 2b).

Fig. 4(a) illustrates the skin friction distribution versus wall suction velocity $(V_C > 0)$ for various values of Da^{-1}. There is a strong decrease in skin friction with increment in suction effect. Similarly, there is a significant reduction produced in skin friction with greater values of Da^{-1}. This parameter which is the inverse Darcy number features in the linear Darcian impedance term, $-(\delta_2 Da^{-1}) f_\eta$ in the transformed momentum Eqn. (10). As Da^{-1} increases, i.e. the medium possesses lower permeability so that there are more solid fibers of the porous matrix. The Darcian drag force is therefore elevated and this generates a concomitant deceleration in the transverse flow manifesting in depletion in the skin friction at the coating surface. Momentum boundary layer thickness is therefore increased with increment in inverse Darcy number, Da^{-1}. However despite the marked retardation induced in the transverse flow, backflow is never caused i.e. there is no change in polarity of the skin friction. The suction effect clearly causes significant

adherence of the momentum boundary layer in the nanofluid flow to the sheet (wall) surface. Again however it does not produce flow reversal. The case of $V_C = 0$ corresponds to a solid wall i.e. absence of perforations and clearly results in the maximum skin friction computed. Effectively therefore strong wall suction and lower permeability of the porous medium successfully damp the boundary layer flow and this is advantageous in flow control operations in nanofluid materials processing as noted by Shukla *et al.* [44], among others. In all cases, skin friction gradually decays in the free stream and asymptotically smooth profiles are computed confirming that a sufficiently large infinity boundary condition has been imposed in the computations. Fig. 4(b) depicts the evolution in skin friction as the function of magnetic parameter, M for various values of V_C. A very sharp decrement is observed initially for low values of M and thereafter profiles decay smoothly to the free stream. Significant suppression in skin friction is produced with greater magnetic field effect verifying the earlier results presented for damping with enhanced Lorentz hydromagnetic body force, which is simulated with the term, $-(\delta_3 M) f_\eta$ in Eqn. (10). Again, a strong deceleration in the flow (i.e. depletion in skin friction) is induced with greater suction effect (V_C). Momentum boundary layer thickness is therefore reduced with both elevation in magnetic field and suction, and again both these effects are excellent mechanisms for flow regulation in coating boundary layers.

Fig. 5(a) displays the evolution in concentration field for various M values in the case of suction at the wall $(V_C = 1)$. Although magnetohydrodynamic effects do not feature directly in the concentration Eqn. (11), the term $+Scf_\eta$ couples the nanoparticle concentration, φ_η to the momentum Eqn. (10). Magnetic Lorentz force therefore indirectly influences the nanoparticle species diffusion field which is enhanced with stronger M values. The concentration boundary layer thickness is therefore also elevated with increment in M. In all cases the concentration decays exponentially from the maximum value at the wall $(\eta = 0)$ and converges to zero in the free stream (edge of the boundary layer). Fig. 5(b) the effect of solutal slip S_3 on concentration field; evidently there is a strong decrease in concentration magnitudes with greater solutal slip. The parameter, S_3 features only in the wall concentration boundary condition, $\phi(0) = 1 + S_3 \phi_\eta(0)$. With greater slip there is a delay in mass transfer from the wall to the nanofluid. This

leads to a reduction also in a thinner concentration boundary layer. A similar observation has been made by Shukla *et al.* [50]. The implication is that when solutal slip is either low or ignored, the concentration values are over-predicted as is the concentration boundary layer thickness. Concentration converges to zero more quickly than in previous plot. The 3-D graphs for velocities along *x*- (axial) and *y*- (transverse) directions are shown in Fig. 6 and Fig.7 for both the suction and injection cases. At low values of *y*, *x*-direction velocities are maximized whereas they are minimized at low values of *x (Fig. 6a, suction case)*. In the injection case (Fig. 6b), velocity is maximum at only high values of *x* and low value of *y*. Fig. 7 a shows that with suction, *y*-direction velocity is maximized at large *y* and minimized at *lower values for all x values.* However, with injection*, Fig. 7b* shows a similar topology to *Fig. 7a*, although the profile is more linear rather than the strong parabolic profile in Fig. 7a. The effects of suction and injection are therefore prominently demonstrated in these 3-D profiles.

6. CONCLUSIONS

A mathematical model for HNF boundary layer slip flow and mass transfer from a stretching surface in porous media with the impact of magnetic field and chemical reaction has been developed. Using appropriate transformations, analytical solutions have been derived in terms of exponential and gamma functions for the velocity and concentration field, under appropriate boundary conditions. A parametric study of selected parameters i.e. magnetic body force parameter, inverse Darcy number, wall transpiration (suction and injection) and wall solutal slip on transverse and axial velocity, skin friction and concentration distributions is visualized graphically. The main findings of observed results can be summarized as follows:

- Velocities are decreased and momentum boundary layer thickness is elevated with increasing magnetic field.

- The transverse velocity is always positive while the axial velocity may be negative also depending on the strength of the magnetic field.
- With increasing inverse Darcy number (i.e. decreasing permeability) the velocity is reduced, and momentum boundary layer thickness is enhanced.
- The skin friction is generally suppressed with increasing suction and increased with injection.
- The concentration magnitudes are boosted with magnetic field whereas they are depleted with increasing solutal slip.

The present nanofluid hydromagnetic coating model has shown that the Laplace transform method has many useful applications in nanofluid transport modeling. However, this study has considered only *Newtonian* hybrid nanofluid flow. Future studies may implement *micropolar non-Newtonian models* and will be communicated imminently.

REFERENCES

1. S.K. Das, *Nanofluids: Science and Technology*, CRC Press, Florida (2007).
2. J.C. Umavathi, O. Anwar Bég, R.S.R. Gorla and B. Vasu, Perturbation and MAPLE quadrature computation of thermo-solutal dissipative reactive convective flow in a geothermal duct with Robin boundary conditions, *TFRE 2020: International Conference on Recent Trends in Developments of Thermo-fluids and Renewable Energy, NIT Arunachal Pradesh, Yupia, India, June* 24-26 (2020*).*
3. F. Sagala, T. Montoya, A. Hethnawi, G. Vitale, Nashaat N. Nassar, Nanopyroxene-based nanofluids for enhanced oil recovery in sandstone cores at reservoir temperature, *Energy Fuels,* 33, 2, 877–890 (2019).
4. T.F. Xiu*,* Lun Pan, Fang Wang, Li Wang, Xiangwen Zhang, Ji-Jun Zou, *Al* -nanoparticle-containing nanofluid fuel: synthesis, stability, properties, and propulsion performance, *Ind. Eng. Chem. Res.* 2016, 55, 10, 2738–2745.
5. M. Amrita, RR Srikant, AV Sitaramaraju, MMS Prasad, P Vamsi Krishna, Preparation and characterization of properties of nanographite-based cutting fluid for machining operations,

Proceedings of the Institution of Mechanical Engineers, Part J: Journal of Engineering Tribology, vol. 228, 3: pp. 243-252 (2013).

6. Rashmi W, Ismail A.F, Khalid M, Anuar A, Yusaf T, Investigating corrosion effects and heat transfer enhancement in smaller size radiators using CNT-nanofluids. *J. Mater. Sci.* 2014; 49: 4544–4551.
7. Islam M.R, Shabani B, Rosengarten G. Electrical and thermal conductivities of 50/50 water-ethylene glycol based TIO_2 nanofluids to be used as coolants in PEM Fuel Cells. *Energy Procedia.* 2017; 110:101–108.
8. Jalal R, Goharshadi E.K, Abareshi M, Moosavi M, Yousefi A, Nancarrow P. ZnO nanofluids: Green synthesis, characterization, and antibacterial activity. *Mater. Chem. Phys.* 2010; 121:198–201.
9. Vékás L, Avdeev M.V, Bica D. (2009) Magnetic Nanofluids: Synthesis and Structure. In: Shi D. (eds) NanoScience in Biomedicine. *Springer*, Berlin, Heidelberg. https://doi.org/10.1007/978-3-540-49661-8_25.
10. Moreau. R.: *Magnetohydrodynamics*, Kluwer Academic Publishers (1990).
11. O. Anwar Bég, Ayesha Sohail, T.A. Bég and A. Kadir, B-spline collocation simulation of nonlinear transient magnetic nano-bio-tribological squeeze film flow, *J. Mechanics in Medicine and Biology,* 18, 1850007.1- 1850007.20 (20 pages) (2018).
12. J. Li *et al.* Hard-magnet $L1_0$-CoPt nanoparticles advance fuel cell catalysis, *Joule*,3 (1) 124-135 (2019).
13. MD. Shamshuddin, S.R. Mishra, O. Anwar Bég, T.A. Bég and Ali Kadir, Computation of radiative Marangoni (thermocapillary) magnetohydrodynamic convection in Cu-water based nanofluid flow from a disk in porous media: smart coating simulation, *Heat Transfer* (2020). DOI: 10.1002/htj.21963 (20 pages) .
14. U. S. Mahabaleshwar, P. N. Vinay Kumar, Mikhail Sheremet, Magnetohydrodynamics flow of a nanofluid driven by a stretching/ shrinking sheet with suction, *SpringerPlus,* (2016) 5: 1901.
15. M. Aneja, Sapna Sharma, S. Kuharat and O. Anwar Bég, Computation of electroconductive gyrotactic bioconvection under nonuniform magnetic field: Simulation of smart bio-nanopolymer coatings for solar energy, *Int. J. Modern Physics B,* 33, 2050028 (22 pages). (2020).
16. M.A.A. Hamad, Analytical solution of natural convection flow of a nanofluid over a linearly stretching sheet in the presence of magnetic field, *Int. Comm. Heat Mass Transfer,* 38 (2011) 487-492.
17. K.-L. Hsiao, Micropolar nanofluid flow with MHD and viscous dissipation effects towards a stretching sheet with multimedia feature, *International Journal of Heat and Mass Transfer*, vol. 112, pp. 983–990 (2017).
18. Dhananjay Yadav, U. S. Mahabaleshwar, Abderrahim Wakif, Ramesh Chand, Significance of the inconstant viscosity and internal heat generation on the occurrence of Darcy-Brinkman

convective motion in a couple-stress fluid saturated porous medium: An analytical solution, *ICHMT*, 122 (2021) 105165.

19. T. Gul *et al.,* Magnetic dipole impact on the hybrid nanofluid flow over an extending surface, *Scientific Reports* volume 10, Article number: 8474 (2020).
20. A.M. Rashad, A.J. Chamkha, M.A. Ismael, T. Salah, Magnetohydrodynamics natural convection in a triangular cavity filled with a Cu-Al_2O_3/water hybrid nanofluid with localized heating from below and internal heat generation, *ASME Journal of Heat Transfer*, 140(7) (2018) 072502.
21. Jamshed, W, Aziz, A. Cattaneo–Christov based study of TiO2–CuO/EG Casson hybrid nanofluid flow over a stretching surface with entropy generation. Appl. Nanosci. 2018, 8, 685–698.
22. Rostami, M.N, Dinarvand, S, Pop, I. Dual solutions for mixed convective stagnation-point flow of an aqueous silica–alumina hybrid nanofluid. Chin. J. Phys. 2018, 56, 2465–2478. [CrossRef].
23. L.A. Lund, Z. Omar, I. Khan, E.S.M. Sherif, Dual solutions and stability analysis of a hybrid nanofluid over a stretching/shrinking sheet executing MHD Flow. *Symmetry* 2020, 12, 276.
24. T. Hayat, S. Nadeem, Heat transfer enhancement with Ag-CuO/water hybrid nanofluid. *Results Phys.* 2017, 7, 2317–2324.
25. J. Prakash, D. Tripathi, O. Anwar Bég, Comparative study of hybrid nanofluid performance in microchannel slip flow induced by electroosmosis and peristalsis, *Applied Nanoscience* (2020). (14 pages).*doi.org/10.1007/s13204-020-01286-1***.**
26. Aly, E.H, Pop, I. MHD flow and heat transfer over a permeable stretching/shrinking sheet in a hybrid nanofluid with a convective boundary condition. *Int. J. Numer. Methods Heat Fluid Flow* 2019.
27. Khan, A.S, Khan, M.I, Hayat, T. Faisal Javed, M, Alsaedi, A. Mixed convective non-linear radiative flow with TiO2 -Cu-water hybrid nanomaterials and induced magnetic field. Symmetry 2020, 12, 1513 15 of 16 29.
28. Olatundun, A.T, Makinde, O.D. Analysis of Blasius flow of hybrid nanofluids over a convectively heated surface. In Defect and Diffusion Forum; Trans Tech Publications: Stafa-Zurich, Switzerland, 2017; Volume 377, pp. 29–41.
29. Ju, B, Fan, T, Experimental study and mathematical model of nanoparticles transport in porous media. *Powder Tech*. **192**(2), 195–202 (2009).
30. D. Pal, G. Mandal, Mixed convection–radiation on stagnation-point flow of nanofluids over a stretching/shrinking sheet in a porous medium with heat generation and viscous dissipation, *J. Pet. Sci. Eng*. 126 (2015) 16–25.
31. O. Anwar Bég, Noman Kabir, Uddin M.J, Ahmad Izani Md. Ismail, Yasser AlginahI, Numerical investigation of Von Karman swirling bioconvective nanofluid transport from a rotating disk in a porous medium with Stefan blowing and anisotropic slip effects, *Proc. IMechE- Part C- J. Mechanical Engineering Science (UK). (2020).DOI: 10.1177/0954406220973061 (19 pages).*

32. T.D. Manh, I. Tlili, A. Shafee, T N Thoi, H Hamouda, Modeling of hybrid nanofluid behavior within a permeable media involving buoyancy effect, *Physica A: Statistical Mechanics and its Applications* (2019) 123940.
33. K . Venkatadri, S. A. Gaffar, V. R. Prasad, B. Md. H. Khan and **O.** Anwar Bég, Melting heat transfer analysis of electrically conducting nanofluid flow over an exponentially shrinking/stretching porous sheet with radiative heat flux under magnetic field**,** *Heat Transfer 49 (8), 4281-4303 (2020).*
34. X. Chen *et al.,* Controlling nanomaterial synthesis, chemical reactions and self-assembly in dynamic thin films, *Chem. Soc. Rev.,* 43, 1387-1399 (2014).
35. C.A. Charitidis *et al.,* Manufacturing nanomaterials: from research to industry, *Manufacturing Review,* 1, 11, 1-19 (2014).
36. F. Talay Akyildiz, Hamid Bellout, K. Vajravelu, Diffusion of chemically reactive species in a porous medium over a stretching sheet, *Journal of Mathematical Analysis and Applications,* 320 (2006) 322-339.
37. J.M.N. Abad *et al.,* Analysis of transport processes in a reacting flow of hybrid nanofluid around a bluff-body embedded in porous media using artificial neural network and particle swarm optimization, *Journal of Molecular Liquids*, 313 (2020) 113492.
38. M. J. Uddin, O. Anwar Bég, A. Aziz and A. I. M. Ismail, Group analysis of free convection flow of a magnetic nanofluid with chemical reaction, *Math. Prob. Engineering 2015, Article ID 621503, 11 pp (2015). doi:10.1155/2015/621503.*
39. Fazle Mabood, Stanford Shateyl, Multiple slip effects on MHD unsteady flow heat and mass transfer impinging on permeable stretching sheet with radiation, *Modelling and Simulation in Engineering,* 2019, 3052790.
40. O. Anwar Bég, J. Zueco and L. M. López-Ochoa, Network numerical analysis of optically-thick hydromagnetic slip flow from a porous spinning disk with radiation flux, variable thermophysical properties and surface injection effects, *Chemical Engineering Communications,* 198, 3, 360-384 (2011).
41. U. S. Mahabaleshwar, Ioannis E. Sarris, Giulio Lorenzini, Effect of radiation and Navier slip boundary of Walters' liquid B flow over a stretching sheet in a porous media, *International Journal of Heat and Mass Transfer* 127 (2018) 1327-1337.
42. U. S. Mahabaleshwar, K. R. Nagaraju, M. A. Sheremet, P. N. Vinay Kumar, G. Lorenzini, Effect of mass transfer and MHD induced Navier's slip flow due to a nonlinear stretching sheet, *Journal of Thermophysics*, 2019, Vol. 28, No. 4, pp. 578-590.
43. A.K. Abdul Hakeem, N. Vishnu Ganesh, B. Ganga, Magnetic field effect on second order slip flow of nanofluid over a stretching/shrinking sheet with thermal radiation effect. J. Magn. Magn. Mater., 381 (2015), 243-257.
44. N. Shukla, Puneet Rana, **O.** Anwar Bég, A. Kadir and Bani Singh, Unsteady electromagnetic radiative nanofluid stagnation-point flow from a stretching sheet with chemically reactive nanoparticles, Stefan blowing effect and entropy generation*, Proc. IMechE: Part N-Journal of Nanomaterials, Nanoengineering and Nanosystems, 232, 69-82 (2018).*

45. M. Govindaraju *et al.,* Analysis of slip MHD nanofluid flow on entropy generation in a stretching sheet, *Procedia Engineering*, 127, 501-507 (2015).
46. M.M. Bhatti, C.M. Khalique, Tasveer Bég, O. Anwar Bég and Ali Kadir, Numerical study of slip and radiative effects on magnetic Fe_3O_4-water-based nanofluid flow from a nonlinear stretching sheet in porous media with Soret and Dufour diffusion, *Modern Physics Letters B33, 2050026 (24 pages) (2020).*
47. M. J. Babu and N.Sandeep, 3D MHD slip flow of a nanofluid over a slendering stretching sheet with thermophoresis and Brownian motion effects, *Journal of Molecular Liquids*, 222, 1003-1009 (2016).
48. M.J. Uddin, O. Anwar Bég and N.S. Amin, Hydromagnetic transport phenomena from a stretching or shrinking nonlinear nanomaterial sheet with Navier slip and convective heating: a model for bio-nano-materials processing, *J. Magnetism Magnetic Materials, 368, 252-261(2014).*
49. Ayele Tulu and Wubshet Ibrahim, MHD slip flow of CNT-ethylene glycol nanofluid due to a stretchable rotating disk with Cattaneo–Christov heat flux model, *Math Problems Engineering*, Volume 2020 |Article ID 1374658 (2020).
50. N. Shukla, P. Rana, O. Anwar Bég, Bani Singh and A. Kadir, Homotopy study of magnetohydrodynamic mixed convection nanofluid multiple slip flow and heat transfer from a vertical cylinder with entropy generation, *Propulsion and Power Research (2019). https://doi.org/10.1016/j.jppr.2019.01.005 (16 pages).*
51. Hoda Saleh, Elham Alali, AbdelhalimEbaid, Medical applications for the flow of carbon-nanotubes suspended nanofluids in the presence of convective condition using Laplace transform, *Journal of the Association of Arab Universities for Basic and Applied Sciences, 2017.*
52. Abdelhalim Ebaid, Mohammed A. Al Sharif, Application of Laplace transform for the exact effect of a magnetic field on heat transfer of carbon nanotubes- suspended nanofluids, *Z. Naturforsch,* 2015, 70 (6) a: 471-475.
53. Malkeet Singh Bhullar, Study on properties and applications of Laplace transformation: A review, *Pramana Research Scholar Journal*, Vol 8 , 4, (2018).
54. Mahantesh M. Nandeppanavar, K. Vajravelu, M. Subhas Abel, M. N. Siddalingappa, Second order slip flow and heat transfer over a stretching sheet with non-linear Navier boundary condition, *International Journal of Thermal Science* 58 (2012) 143-150.
55. Lin Wu, A slip model for rarefied gas flows at arbitrary Knudsen number, *Applied Physics Letters,* 93, 253103 (2008).
56. H. I. Andersson, K. H. Bech, Magnetohydrodynamic flow of a power-law fluid over a stretching sheet, *Int. J. Non-Linear Mechanics,* Vo. 27, No. 6, pp. 929-936 (1992).
57. P. G. Siddheshwar, U. S. Mahabaleshwar, H. I. Andersson, A new analytical procedure for solving the non-linear differential equation arising the stretching sheet problem, *Int. J. of Applied Mechanics and Engineering,* 2013, 18, No. 3, pp. 955-964.

58. H. I. Andersson, Olav R. Hansen, Bjorn Holmedal, Diffusion of a chemically reactive species from a stretching sheet, *Int.J. Heat Mass Transfer,* Vol. 37, No. 4, pp. 659-664, 1994.

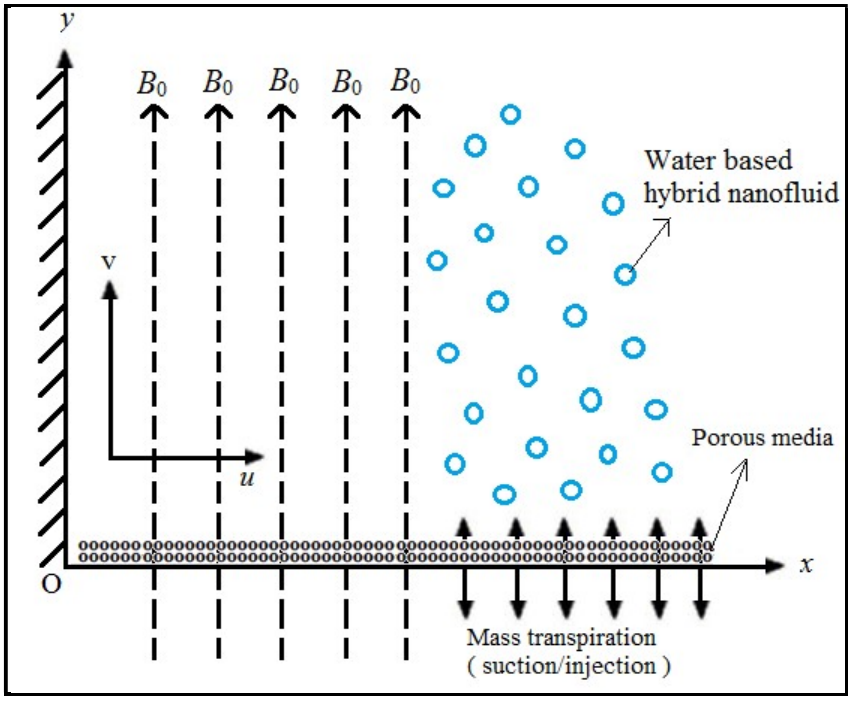

Fig. 1: Schematic of reactive MHD nanofluid coating boundary layer flow in porous media.

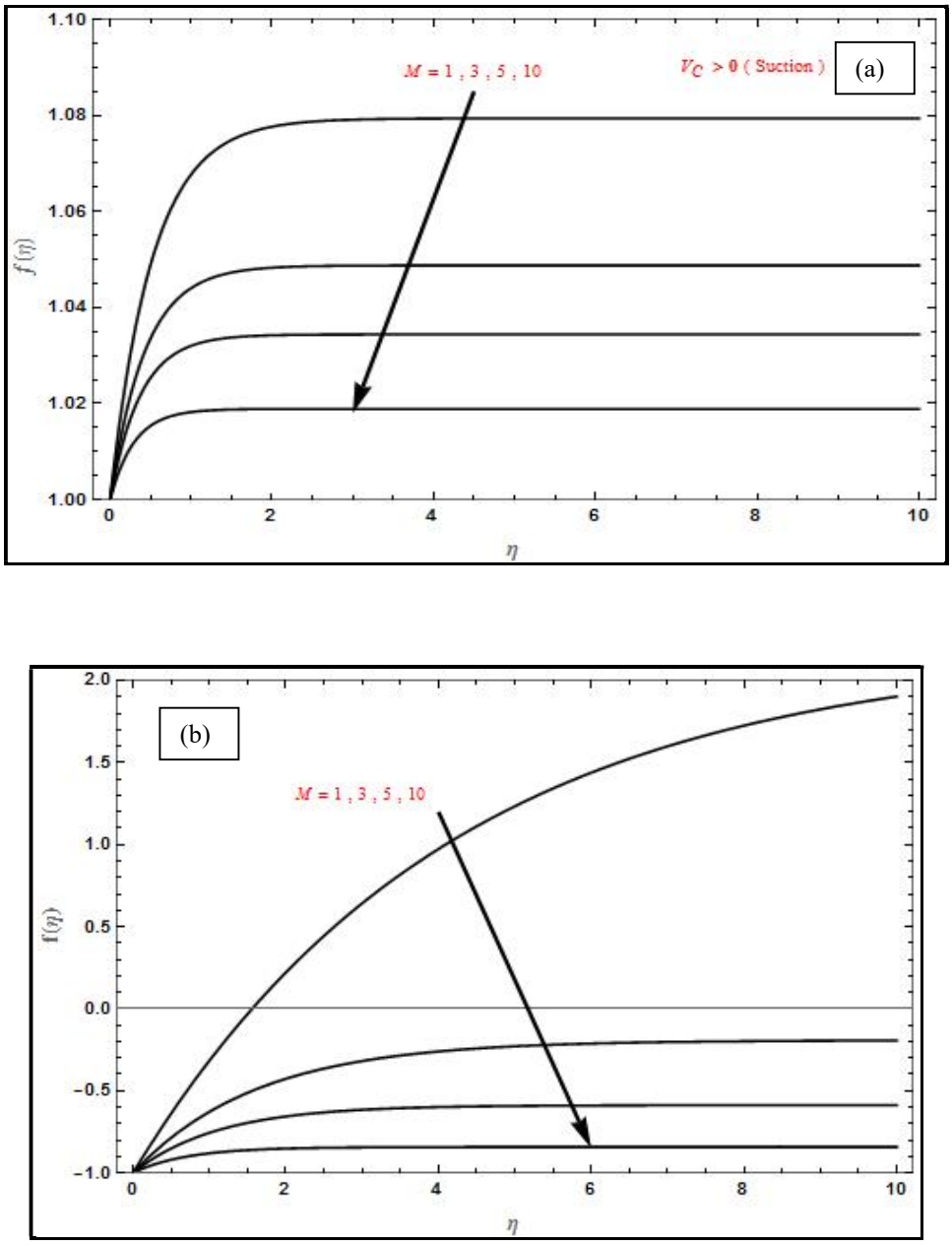

Fig 2: Transverse velocity profile $f(\eta)$ for varying magnetic parameter (M) for (a) suction $(V_C = 1)$ and (b) injection $(V_C = -1)$ with, $Da^{-1} = \Lambda = 1$, $S_1 = 1$, $S_2 = -1$, $\varphi_1 = 0.1$, $\varphi_2 = 0.04$.

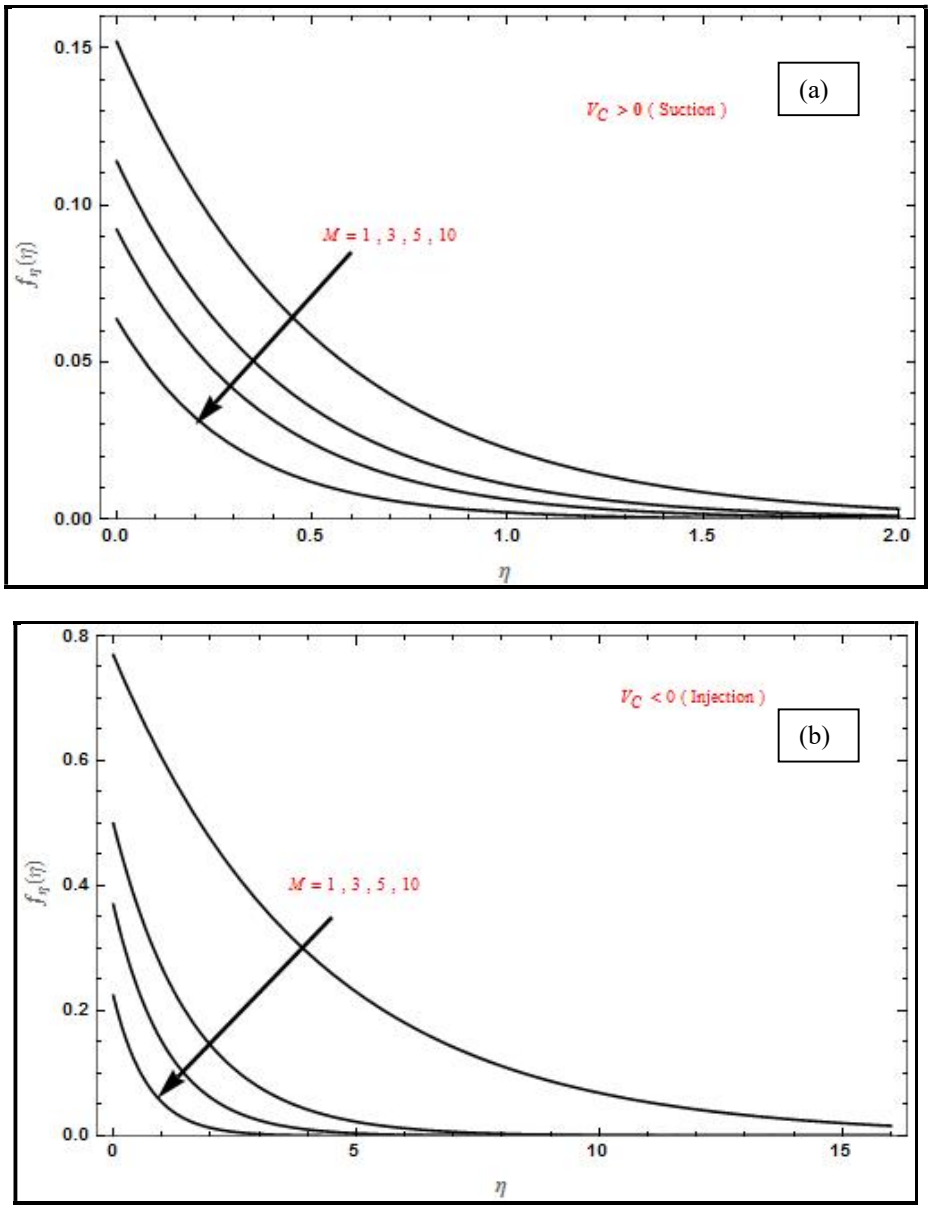

Fig 3: Axial velocity profile $f_\eta(\eta)$ for varying magnetic parameter (M) for (a) suction $(V_C = 1)$ and (b) injection $(V_C = -1)$ with $Da^{-1} = \Lambda = 1$, $S_1 = 1$, $S_2 = -1$, $\varphi_1 = 0.1$, $\varphi_2 = 0.04$.

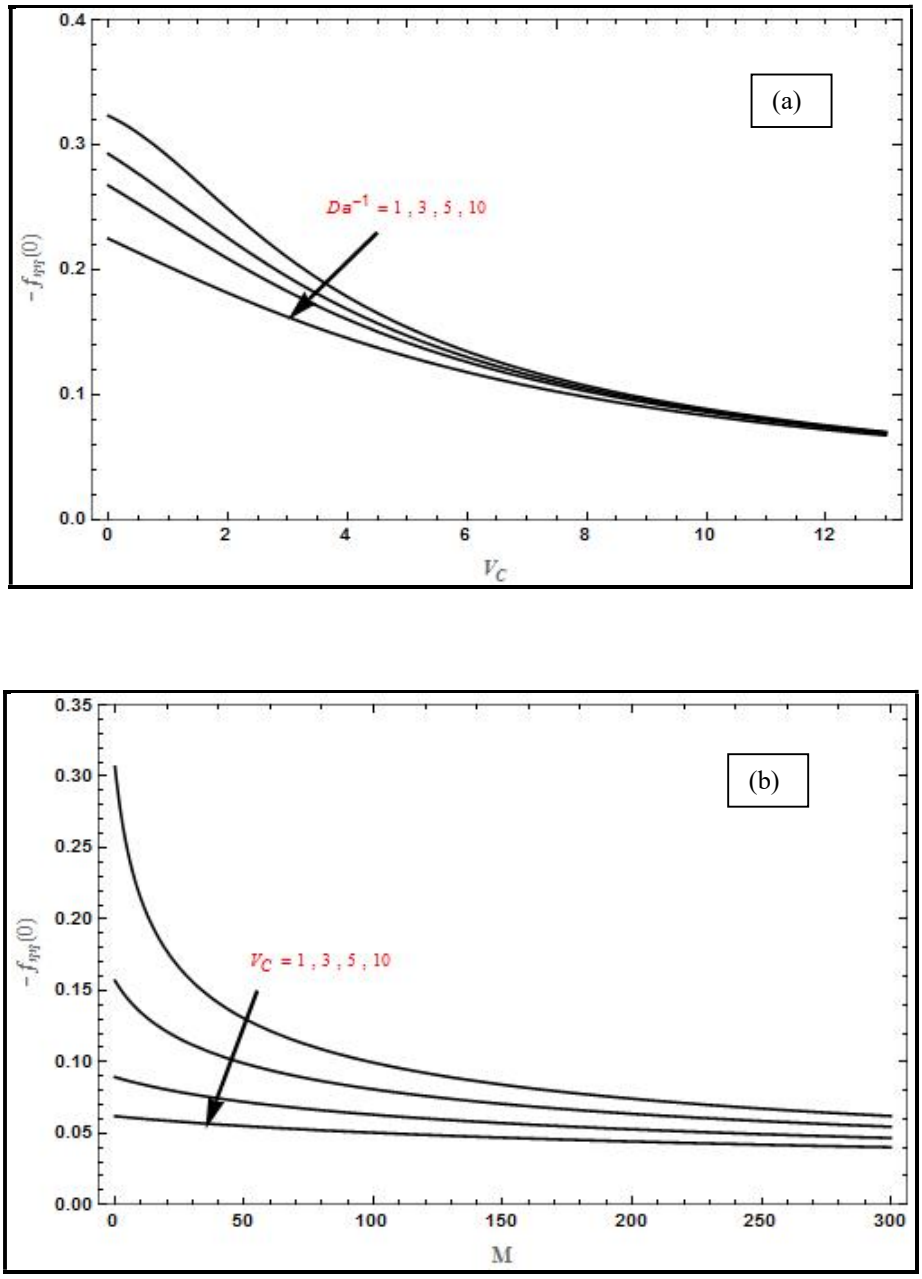

Fig 4: The variation of skin friction $-f_{\eta\eta}(0)$ in (a) as a function of V_C for varying value of $\left(Da^{-1}\right)$ with $M=1$ and in (b) as a function of M for varying values of V_C with $Da^{-1}=1$ and $\Lambda=1, S_1=1$, $S_2=-1$, $\varphi_1=0.1$, $\varphi_2=0.04$.

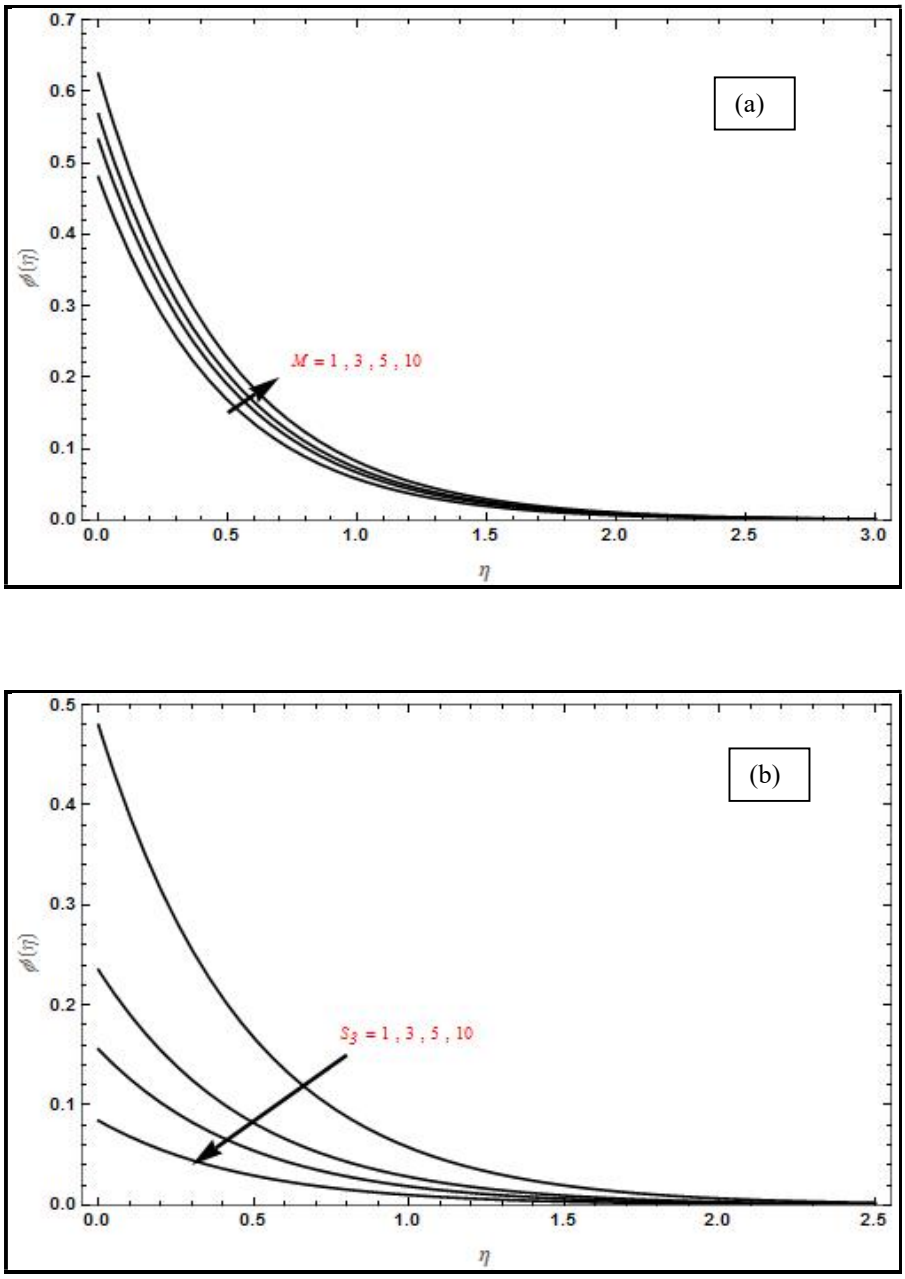

Fig 5: Concentration profile $\phi(\eta)$for varying values of (a) magnetic parameter $(M)$with $S_3 = 1$ and in (b) for varying values of S_3 with $M = 1$ for suction case $(V_C = 1)$ with $Da^{-1} = \Lambda = 1, Sc = 2, S_1 = 1, S_2 = -1, \varphi_1 = 0.1, \varphi_2 = 0.04.$

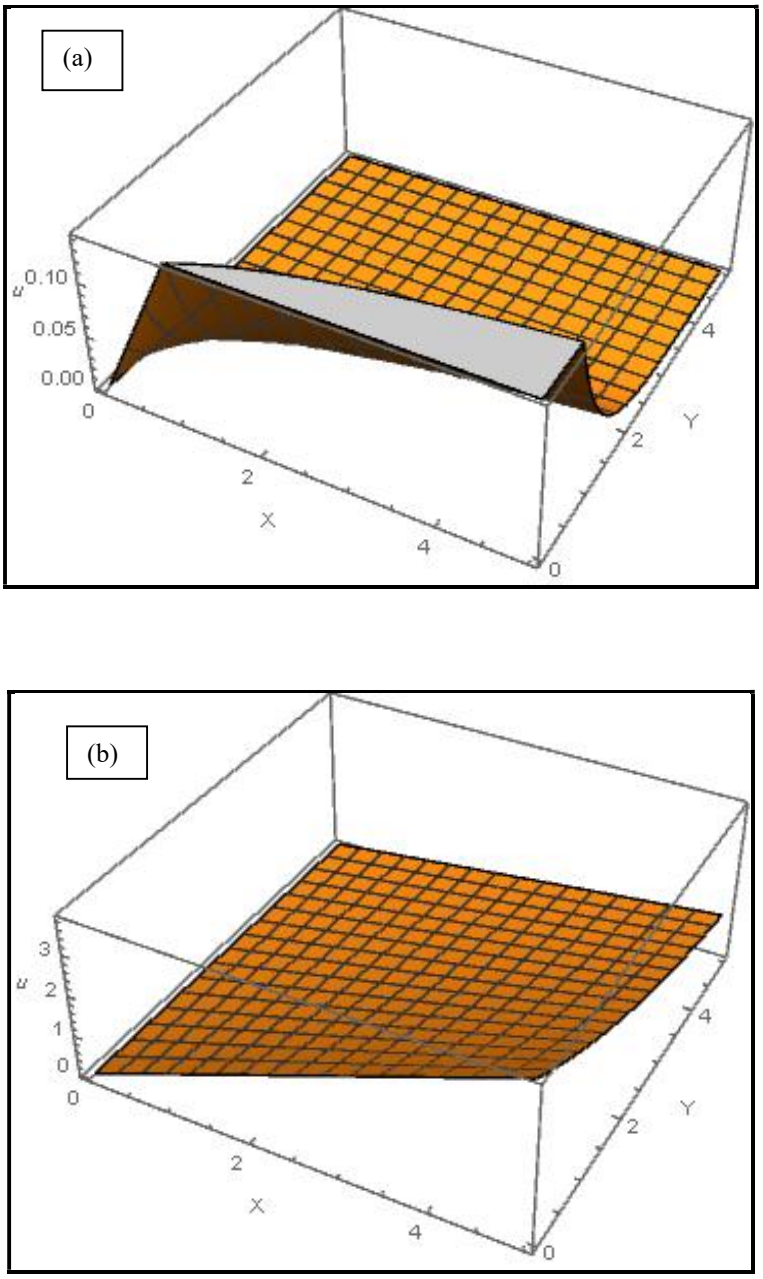

Fig 6: 3-D graph of velocity profile along *x*-direction for (a) suction case $(V_C = 1)$ and (b) injection case $(V_C = -1)$ with $M = Da^{-1} = \Lambda = 1, S_1 = 1$, $S_2 = -1$, $\varphi_1 = 0.1$, $\varphi_2 = 0.04$.

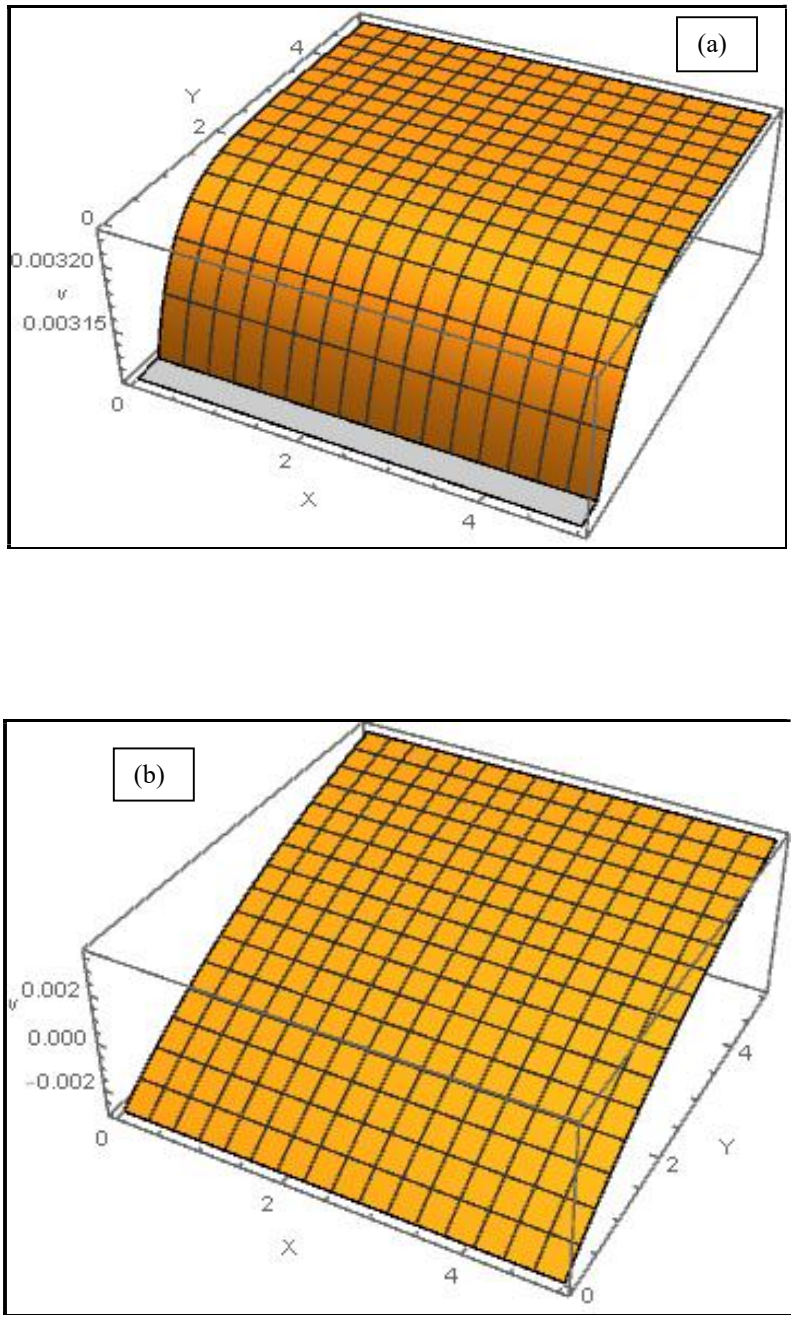

Fig 7: 3-D graph of velocity profile along *y*-direction for (a) suction case $(V_C = 1)$ and (b) injection case $(V_C = -1)$ with $M = Da^{-1} = \Lambda = 1, S_1 = 1, S_2 = -1, \varphi_1 = 0.1, \varphi_2 = 0.04.$

Nomenclature

Latin symbols

a	constant
A, B	constants
B_0	applied magnetic field
C	nanoparticles concentration field
C_w	wall concentration
C_∞	concentration away from the wall
D_B	solutal diffusivity
Da^{-1}	inverse Darcy number $\left(=\frac{\nu_f}{\kappa a}\right)$
f	similarity variable
k_c	rate constant of chemical reaction
K	Knudsen number
K_1, L_1, L_2	slip parameter functions
M	magnetic interaction parameter $\left(=\frac{\sigma_f B_0^2}{\rho_f a}\right)$
$S_1 \geq 0$	first order momentum slip parameter
$S_2 \leq 0$	second order momentum slip parameter
S_3	solutal slip parameter
Sc	Schmidt number $\left(=\frac{\nu_f}{D_B}\right)$
u , v	velocity along x- and y- direction
V_C	mass transpiration parameter

v_w	wall mass transfer velocity
x , y	co-ordinate axes

Greek symbols

α	molecular free path
β	$\left(=\frac{k_c}{a}\right)$ chemical reaction parameter
γ	coefficient of momentum accommodation
δ_1	density ratio $\left(=\frac{\rho_{hnf}}{\rho_f}\right)$
δ_2	dynamic viscosity ratio $\left(=\frac{\mu_{hnf}}{\mu_f}\right)$
δ_3	electrical conductivity ratio $\left(=\frac{\sigma_{hnf}}{\sigma_f}\right)$
η	similarity variable(dimensionless transverse coordinate)
κ	permeability of porous medium
λ	exponent
μ	dynamic viscosity
ν	kinematic viscosity
ν_{eff}	$\left(=\frac{\mu_{eff}}{\rho_f}\right)$ effective kinematic viscosity
ξ	change of variable
ρ	density
σ	electrical conductivity
ϕ	similarity variable for concentration
ψ	stream function
Γ	incomplete gamma function

Λ	$\left(=\frac{\mu_{eff}}{\mu_f}\right)$ Brinkman viscosity ratio

Subscripts

f	parameter of base fluid
hnf	parameter of hybrid nanofluid

Abbreviations

BC	boundary conditions
CNTs	carbon nanotubes
HNF	hybrid nanofluid
L.T	Laplace transformation
MHD	magnetohydrodynamics
NF	nanofluid
ODEs	ordinary differential equation
PDEs	partial differential equations